# Conformation and Hydrogen Bonding Properties of an Aziridinyl Peptide: X-ray Structure Analysis, Raman Spectroscopy and Theoretical Investigations

**10 AUTHORS**, INCLUDING:

Adriana Szeghalmi
Friedrich Schiller University Jena
**51** PUBLICATIONS **731** CITATIONS

SEE PROFILE

Michael Schmitt
Universität Heidelberg
**277** PUBLICATIONS **5,516** CITATIONS

SEE PROFILE

Wolfgang Kiefer
University of Wuerzburg
**878** PUBLICATIONS **9,847** CITATIONS

SEE PROFILE

# Conformation and Hydrogen Bonding Properties of an Aziridinyl Peptide: X-ray Structure Analysis, Raman Spectroscopy and Theoretical Investigations

**Tanja Schirmeister,**[*,†] **Alexander Breuning,**[†] **Alexander Murso,**[‡] **Dietmar Stalke,**[*,‡]
**Milena Mladenovic,**[§] **Bernd Engels,**[*,§] **Adriana Szeghalmi,**[‖] **Michael Schmitt,**[‖,⊥]
**Wolfgang Kiefer,**[‖] **and Jürgen Popp**[*,⊥]

*Institute of Pharmacy and Food Chemistry, University of Würzburg, Am Hubland,*
*D-97074 Würzburg, Germany, Institute of Inorganic Chemistry, University of Würzburg, Am Hubland,*
*D-97074 Würzburg, Germany, Institute of Organic Chemistry, University of Würzburg, Am Hubland,*
*D-97074 Würzburg, Germany, Institute of Physical Chemistry, University of Würzburg, Am Hubland,*
*D-97074 Würzburg, Germany, and Institute of Physical Chemistry, University of Jena, Helmholtzweg 4,*
*D-07743 Jena, Germany*

*Received: July 6, 2004; In Final Form: September 15, 2004*

The X-ray structure analysis of the aziridinyl peptide EtO-Azi-Gly-Gly-OBn indicates that the linear conformation adopted in the crystalline state is established by an intermolecular hydrogen bonding network. This is confirmed by force field computations. They show that the intermolecular interactions in the crystal are stronger than the intramolecular ones which for a single molecule would lead to a bent structure. As expected, the stabilization energies strongly decrease with increasing polarity of the environment. For medium polar environments, the intermolecular interactions are still stronger than the intramolecular ones which is in nice agreement with results from $^1$H NMR dilution studies in CDCl$_3$. For very polar environments, the intramolecular interactions become stronger than the intermolecular ones, however, if the solvent is able to form stable hydrogen bonds, e.g., DMSO, the intramolecular hydrogen bonds are replaced by hydrogen bonds to the solvent molecules. Raman spectra of the crystalline compound prove that the aziridine NH as well as the peptide bonds are involved in hydrogen bonding.

## Introduction

In the past few years, the interest in inhibitors of cysteine proteases has increased considerably.[1–3] Since these proteases play essential roles in various pathological processes, low molecular weight inhibitors could be useful therapeutic agents. One class of inhibitors comprises peptides containing an epoxide[4–8] or an aziridine[9–14] ring. These three-membered heterocycles act as electrophilic "war heads" which can be attacked by the cysteine residue of the enzyme's active site thus leading to irreversible enzyme alkylation and inactivation (Figure 1). Until now, no X-ray-crystallographic structure of peptides containing the aziridine-2,3-dicarboxylic acid as electrophilic amino acid has been determined, and neither do structures of enzyme–inhibitor complexes exist.[15] This is in contrast to the oxygen analogues of these inhibitors, the epoxysuccinyl peptides, for which the X-ray crystallographic structure of the prototype inhibitor loxistatin (Figure 1)[16] as well as a variety of 3D-structures of enzyme–inhibitor complexes have been determined.[17]
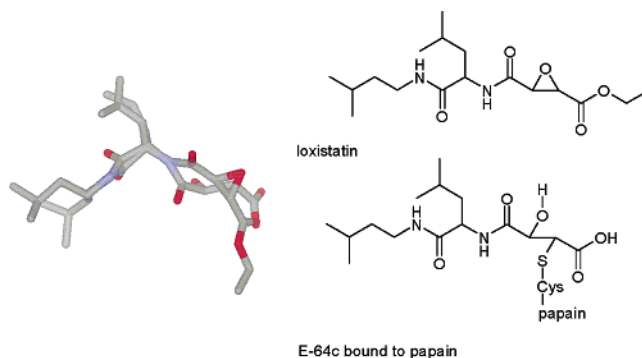


**Figure 1.** Overlay of the structure of the ethyl ester loxistatin[16] with its active open-chain acid E−64c taken from the complex with papain (1PE6).[17f]

To understand the different binding modes of these related inhibitor types, the preferred conformations have to be known. In addition, the knowledge of inter- and intramolecular hydrogen bonding motifs can contribute to a better understanding of structure–activity relationships. With the X-ray structure determination of ethyl-(2*S*,3*S*)-3-{[2-{[benzyloxy)-2-oxoethyl]-amino}-2-oxoethyl)amino]carbonyl}aziridine-2-carboxylate (EtO-Azi-Gly-Gly-OBn) (**2**; Figure 2), Raman-spectroscopic studies, force field as well as quantum chemical calculations of this aziridinyl peptide and its electrophilic building block (diethyl-(2*S*,3*S*)-aziridine-2,3-dicarboxylate, EtO-Azi-OEt) (**1**; Figure 2), we present insights into the conformation and H-bonding properties of this inhibitor type.

* To whom correspondence should be addressed. Syntheses, NMR spectroscopy (T.S.): Phone: ++49 (0) 931 888 5440. E-mail: schirmei@ pzlc.uni-wuerzburg.de. X-ray structure analysis (D.S.): Phone ++49 (0) 931 888 4783. E-mail: dstalke@chemie.uni-wuerzburg.de. Raman spectroscopy (J.P.): Phone ++49 (0) 3641 948320. E-mail: juergen.popp@ uni-jena.de. Theoretical investigations (B.E.): Phone ++49 (0) 931 888 5394. E-mail: engels@chemie.uni-wuerzburg.de.
† Institute of Pharmacy and Food Chemistry, University of Würzburg.
‡ Institute of Inorganic Chemistry, University of Würzburg.
§ Institute of Organic Chemistry, University of Würzburg.
‖ Institute of Physical Chemistry, University of Würzburg.
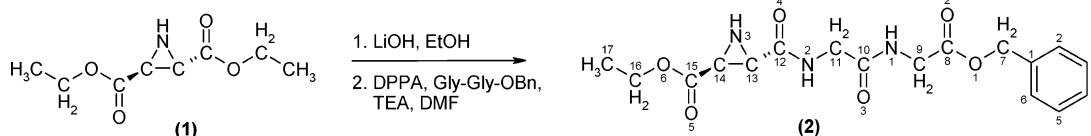⊥ Institute of Physical Chemistry, University of Jena.

Properties of an Aziridinyl Peptide

*J. Phys. Chem. A, Vol. 108, No. 51, 2004* **11399**



**Figure 2.** Synthesis and structure of the aziridinyl peptide EtO-Azi-Gly-Gly-OBn (**2**).

The geometrical structures of the most stable conformers of a single aziridinyl peptide molecule in various environments (gas phase, chloroform, and water) were studied by means of conformational search with MacroModel8.0[18] program starting from the X-ray structure. The intramolecular interactions stabilizing the conformers were analyzed and compared with the intermolecular forces in the crystal considering environments of different polarity. To investigate the behavior of the aziridinyl peptide in the presence of solvents which are able to form hydrogen bonds to the solute, computations with 1−5 molecules of DMSO were undertaken. The accuracy of various force fields was investigated by means of quantum chemical calculations. NMR dilution studies differentiating between intra- and inter-molecular hydrogen bonding were performed to verify the predictions of the calculations.

It is well established that the carbonyl stretching wavenumber is a measure of hydrogen bonding interaction since strong hydrogen bonding leads to a decrease in its wavenumber value.[19] Moreover, the position of the NH stretching modes in vibrational spectra also reflects the H-bonding strength. Furthermore, since an indepth understanding of the structure sensitive amide bands is of high interest,[20] we performed a detailed vibrational analysis on the title compound (**2**) paying special attention to the contribution of the atomic displacements to the normal co-ordinates.

## Experimental Section

**NMR Dilution Experiments with (2).** NMR spectra were recorded in CDCl$_3$ on a Bruker Avance 400 MHz spectrometer. The enumeration of the atoms can be taken from Figure 2. $\delta$ (ppm): at 60 mM concentration:N1H 6.68; N2H 7.12; N3H (aziridine) 1.84; at 30 mM concentration:N1H 6.48; N2H 7.01; N3H (aziridine) 1.83; at 0.3 mM concentration:N1H 6.34; N2H 6.99; N3H (aziridine) 1.79.

**X-ray Structure Determination of (2).** Data were collected at 100(2) K[22] using graphite monochromated Mo Kα radiation ($\lambda = 0.71073$ Å) on a Bruker D8 goniometer platform, equipped with a Smart Apex CCD detector. Cell parameters were determined and refined using the SMART software.[23] Series of $\omega$-scans were performed at several $\phi$-settings. Raw frame data were integrated using the SAINT program.[24] The data were empirically absorption corrected with SADABS 2.05.[25] The structures were solved using direct methods and refined by full-matrix least squares on F$^2$ using SHELXTL.[26] R values defined as $R1 = \Sigma||F_o| - |F_c||/\Sigma|F_o|$, $wR2 = [\Sigma w(F_o^2 - F_c^2)^2/\Sigma w(F_o^2)^2]^{0.5}$, $w = [\sigma^2(F_o^2) + (g_1P)^2 + g_2P]^{-1}$, $P = 1/3$ [max-$(F_o^2,0) + 2F_c^2$].

The positions of the hydrogen atoms were taken from the difference Fourier map and refined freely. All non hydrogen atoms were refined anisotropically. The anisotropic displacement parameters (ADP) in the Supporting Information were drawn at the 50% probability level. Crystallographic data (excluding structure factors) for the structure reported in this paper have been deposited with the Cambridge Crystallographic Data Centre as supplementary publication CCDC−No. 234581. Copies of the data can be obtained free of charge on application to CCDC,

12 Union Road, Cambridge CB2 1EZ, UK [fax: (internat.) + 44(1223)336−033; e-mail: deposit@ccdc.cam.ac.uk].

**2.** C$_{17}$H$_{21}$N$_3$O$_6$, M$_r$ = 363.37 g/mol, monoclinic, space group $P2_1$, $a$ = 4.8094(6), $b$ = 22.453(3), $c$ = 8.3634(10) Å, $\beta$ = 101.212(2)°, $V$ = 885.88(18)Å$^{-3}$, $Z$ = 2, $\rho_{calcd}$ = 1.362 Mgm$^{-3}$, $\mu$ = 0.104 mm$^{-1}$, $F(000)$ = 384. Data were collected from $\theta$ = 1.81 to $\theta$ = 28.06°. 8265 reflections measured, from which 6729 were unique, $R$(int) = 0.0166, $wR2$(all data) = 0.0864, $R1(I > 2\sigma(I))$ = 0.0396, for 3850 data, 1 restraint and 320 parameters. The Flack-x parameter[27] refined to 1.1(9). Largest diff. peak 0.279 e. Å$^{-3}$ and hole −0.216e. Å$^{-3}$.

**Computational Details, MacroModel/XCluster Calculations.** The MacroModel8.0 program package was used for energy minimization of X-ray structures, generation, multiple minimization, and investigation of different conformers of the aziridinyl peptide. The overall computations are divided into three parts.

*1. Minimization of the X-ray Structure.* X-ray experiments often underestimate the length of X−H bonds (X = heavier element). Therefore, to obtain reliable estimates of the interactions within the crystals, it was necessary to perform a geometry optimization. This was performed by a minimization of a part of the crystal consisting of 117 molecules of the aziridinyl peptide. The optimization was started from the X-ray geometry. This part represents a box consisting of 5 layers with approximately 25 molecules in each. The geometries of the molecules in the outer shell were frozen while the geometries of the most inner nine molecules were optimized. MMFF94s force field was used for the energy minimization of the starting X-ray crystal structures and multiple minimizations of the generated conformers. The truncated Newton−Raphson conjugate gradient (TNCG)[28] method was used, while the derivative convergence criterion was set to 0.05 kJ/Åmol, with 5000 as the maximum number of iterations. In the multiple minimizations, all of the atoms were compared. To simulate the influence of polar and medium surroundings the generalized Born/solvent accessible surface[29] (GB/SA) solvent model was used. For polar environments we employed the parametrization made for water while the one for chloroform was used to mimic the influence of medium polar environments.

*2. Conformational Search.* An exhaustive conformational search was performed using the MMFF94s force field. Calculations were done for the molecule in the gas phase as well as for water and chloroform surroundings for which the GB/SA solvent model was used. In all cases, nonbonded cutoffs were set to infinity. For the energy minimization of the generated conformers the TNCG method was used, while the derivative convergence criterion was set to 0.05 kJ/Åmol, with 5000 as the maximum number of iterations. Conformational search was done by random variation of all rotatable bonds by means of mixed Monte Carlo multiple minimum[30] (MCMM)/low mode[31] method. For each calculation 10.000 Monte Carlo steps were performed.

*3. XCluster Calculations.* The XCluster program as a part of the MacroModel8.0 program package was used for clustering and comparison of the generated conformers. The clustering was based on atomic RMSD (root-mean-square distance)
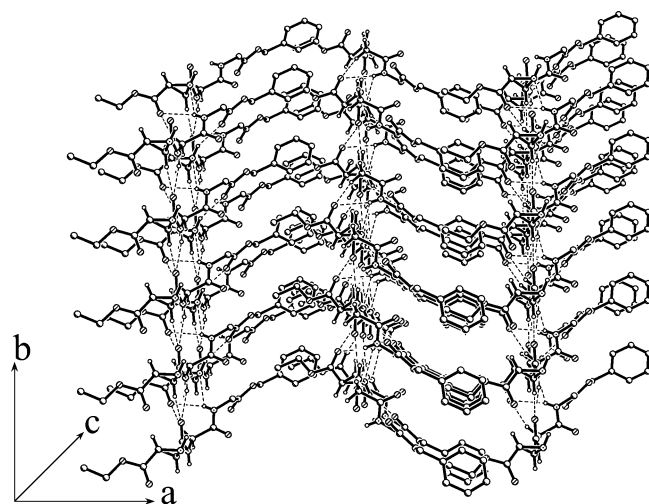
**Figure 3.** Crystal packing of EtO-Azi-Gly-Gly-OBn (**2**).



**Figure 4.** Hydrogen bonding network linking molecules along the crystallographic *c* axis (top) and along the *b* axis (bottom).



**Figure 5.** Head-to-tail connection of the molecules.

**TABLE 1: Hydrogen Bonding in (2)**[a]

| D-H···A[b] | d(D−H) | d(H···A) | d(D···A) | D−H−A |
|---|---|---|---|---|
| C11d−H11d···O5a | 0.91(2) | 2.49(2) | 3.250(2) | 140.5(17) |
| C13a−H13a···O4c | 0.93(2) | 2.55(2) | 3.332(2) | 142.2(17) |
| N1d−H20d···O5a | 0.81(2) | 2.32(2) | 3.084(2) | 158(2) |
| N1d−H20d···N3a | 0.81(2) | 2.56(2) | 3.133(2) | 129.3(18) |
| N2a−H21a···O4c | 0.84(3) | 2.05(3) | 2.864(2) | 163(2) |
| N3a−H22a···O2b | 0.88(2) | 2.16(2) | 2.985(2) | 156.2(18) |

[a] Bond lengths in angstroms and angles in degrees. [b] D = donor, A = acceptor.

differences of certain atoms. To separate conformers with N1−O4 hydrogen bond from the others, clustering of all of the conformers was done in respect to the atoms in the backbone that take part in forming of this bond, namely C10, C11, C12, N1, N2, O4 and an involved hydrogen.

**Raman Spectroscopy.** The Raman spectra excited at 1064 nm (Nd:YAG laser) were recorded with a Fourier transform (FT) spectrometer (Bruker, model IFS120HR) equipped with a Raman module (model FRA106). Detection was achieved with a liquid nitrogen cooled Ge detector. The spectral resolution is 1 cm$^{-1}$. The aziridinyl peptide (**2**) has been investigated in the solid state, whereas **1** has been measured as a fluid. Due to the low solubility of **2** no spectra in solution could be obtained.

## Results and Discussion

**Inhibitor Syntheses.** The electrophilic building block was synthesized by a well-established procedure.[21] Hydrolysis with LiOH led to the half ester which was coupled to the model peptide Gly-Gly-OBn by the DPPA (diphenyl phosphorazidate) procedure (Figure 2).[11] Purification by column chromatography and crystallization from CHCl$_3$ yielded the aziridinyl peptide as colorless needles. A detailed description of the synthesis and the analytical data are included in the Supporting Information.

**Structure Discussion.** The tripeptide (**2**) crystallizes in the chiral monoclinic space group *P*2$_1$. As the bonding parameters are in the range generally observed for organic molecules, the molecular structure, crystallographic tables, and full bond lengths and angles for **2** are only given in the Supporting Information.

In the solid state, the molecules are arranged in zigzag chains and stacked along the crystallographic axes *b* and *c*. Additionally, the ethoxy-substituents interlock between two neighboring phenyl groups along the *a* axis. (Figure 3).

Figure 4 depicts the intermolecular hydrogen bonding network, linking the straight molecules. The hydrogen bonding parameters are presented in Table 1.

Along the *c* axis, the molecules are linked by bifurcated hydrogen bonds between the acceptor O4c and the hydrogen atoms H13a at the aziridine ring atom C13a and H21a at the peptide group containing N2a (the enumeration of the various atoms can be taken from Figure 2). This hydrogen bonding links the middle section of the straight molecules (Figure 4, top). Along the *b* axis, three hydrogen bonds are established between the molecule stacks (atoms indexed a and d). The bifurcated hydrogen bond of the acceptor O5a links the acidic hydrogen atoms H11d at C11d, next to the peptide group at N2d and the
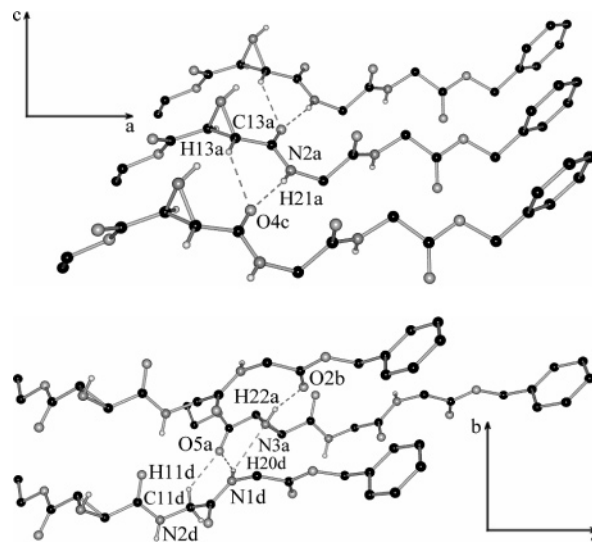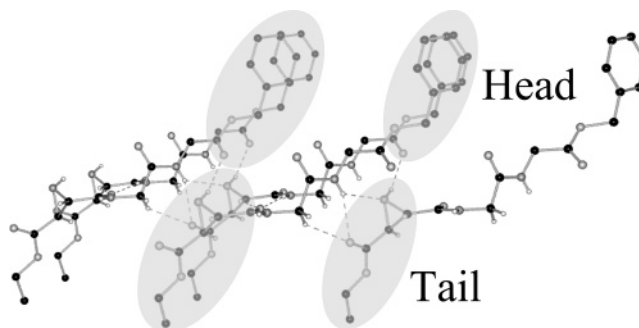
H20d hydrogen atom at N1d. The latter group is a bifurcated donor, as the hydrogen atom H20d additionally binds to the aziridine nitrogen atom N3a. Remarkably, this ring nitrogen atom N3a is not only an H-acceptor but also acts as a donor, because the connected H22a atom is linked to the O2b atom of another molecule. Thus, along the *b* axis one molecule bridges two others, forming four hydrogen bonds (Figure 4, bottom). Interestingly, the hydrogen bonds link the chains in a head-to-tail arrangement (Figure 5).

All of these findings suggest, that this arrangement induces the molecules to adopt this chain like a layered structure.

To classify the different types of hydrogen bonds[32] the definition according to Jeffrey[33] is used. The angles D−H···A vary from 129.3(18)° for N1d−H20d···N3a to 163(2)° for N2a−H21a···O4c. Thus, they all have a moderately strong directional preference. The N−H···O interactions fall in the range from 2.05(3) to 2.32(2) Å and are therefore considered as moderately strong hydrogen bonds. The C−H···O bond lengths vary from 2.49(2) to 2.55(2) Å. As the C···O distances (3.250(2) Å for
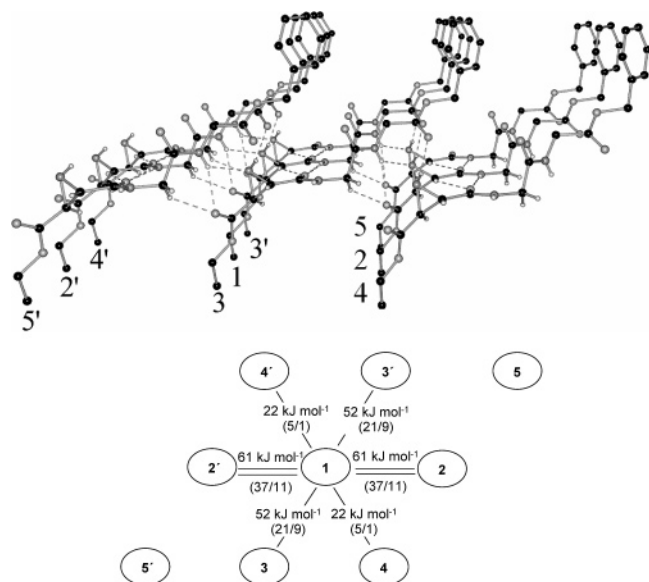
Properties of an Aziridinyl Peptide

*J. Phys. Chem. A, Vol. 108, No. 51, 2004* **11401**



**Figure 6.** Molecules of the aziridinyl peptide crystal used for the calculation of binding energies. Upper part: side view of the crystal structure, intermolecular H-bonds are marked by dotted lines. Lower part: Schematic representation of the top view of the crystal structure with depicted strengths of interactions (numbers in brackets correspond to binding energies in chloroform and water environments, respectively, and are in kJ mol$^{-1}$) and positions and number of H bonds (one line represents one H-bond, two lines two H bonds).

**TABLE 2: Characterization of the Intramolecular Interactions Stabilizing the Bent Structure of a Single Aziridinyl Peptide Molecule in Different Surroundings**

| solvent | stabilization energy[a] (kJ mol$^{-1}$) | no. of the conformers[b] | no. of molecules with N1—O4 H bond (%) | average length of the N1—O4 H bond (Å) |
|---|---|---|---|---|
| gas phase | −82 | 118 | 75 | 2.0 |
| chloroform | −66 | 372 | 51 | 2.2 |
| water | −53 | 386 | 12 | 2.4 |

[a] Stabilization with respect to the linear form adopted in the crystal. [b] Number of the conformers within the limit of 20 kJ mol$^{-1}$ from the most stable conformer.

C11d···O5a and 3.332(2) Å for C13a···O4c) are longer than the suggested value for weak hydrogen bonds (3.2 Å),[33] these interactions seems to be weak. In addition, the N1d—H20d···N3a hydrogen bond has to be regarded a weak interaction, as the distances and angles are 2.56(2) Å for N1d—H20a···N3a, 3.133(2) Å for N1d···N3a, and 129.3(18)° for N1d—H20d···N3a.

In contrast to the related epoxide containing loxistatin (Figure 1),[16] which adopts a flattened, curved conformation in the crystalline state, the solid-state structure of **2** features intermolecular hydrogen bonds inducing the molecules to be arranged in zigzag chains. The epoxide molecules are arranged as a series of infinite parallel $\beta$-sheet structures formed via intermolecular N—H···O hydrogen bonds between the respective N atoms of the two amide groups and the O atoms of the same groups of the neighboring molecule.[16] These H bonds are also formed in the aziridinyl peptide, but additionally, the aziridine-N is also involved in H-bonding as donor and acceptor which is not the case with the oxygen of the epoxide ring of loxistatin.

**Theoretical Investigations.** As a first goal of our theoretical investigations, we studied the intermolecular binding energies in the crystal. They were obtained by single-point calculations on previously minimized geometries starting from solid-state coordinates from the X-ray structures (see computational methods part) which are depicted in Figure 6.

Within the crystal, the strongest interaction appears between the molecules 1 and 2 or 3 and 4, etc. For the corresponding dimers, a binding energy of 61 kJ mol$^{-1}$ is computed for an unpolar environment (e.g., the gas phase), whereas for a polar one, a binding energy of 11 kJ mol$^{-1}$ is predicted. The binding mainly stems from two intermolecular hydrogen bonds with a calculated distance of 2.21 Å for N1H—O5 and 2.83 Å for N1H—N3. The binding energies between two molecules of one column (e.g., 3 and 1 or 1 and 3′) are computed to be 52 kJ mol$^{-1}$ in the gas phase and 9 kJ mol$^{-1}$ in a polar environment. This binding mainly results from the existence of one intermolecular H bond (N1H—O4, 1.82 Å) and from van der Waals

interactions between the $\pi$ systems of the phenyl rings. Weaker interactions are found between molecules in positions that correspond to those of molecules 1 and 4 or 4′. They are computed to be about 22 kJ mol$^{-1}$ in gas phase and only 1 kJ mol$^{-1}$ in an environment being similar polar as water. All other intermolecular interactions (e.g., between 1 and 5 or 5′) are even weaker. As expected from the linear form of the single molecules also intramolecular interactions are neglectable.

The interaction energies discussed above are obtained from dimer calculations. To obtain information about cooperative effects, we computed the total binding energies of various subunits and compared them with the values obtained by summing up the corresponding binding energies of the dimers. For a tetramer consisting of the molecules 1−4, we obtained a total binding energy of 251 kJ mol$^{-1}$. It is nearly identical to the estimate of 248 kJ mol$^{-1}$ which results from summing up the binding energies of the corresponding dimers (1−2, 3−4, 1−3, 4−2, 4−1, see Figure 6 for the energies). For other subunits (up to hexamers) similar results are found. Since cooperative effects seem to be small in the crystal, the interactions between one molecule and all of its neighbors can be estimated to be about 270 kJ mol$^{-1}$. Cooperative effects cannot be estimated in a similar way for solvent models since for the tetramer the intermolecular hydrogen bonds, e.g., between 1 and 2 or 3 and 4 are shielded differently against the continuum than in the corresponding dimers.

To investigate possible conformers of a single aziridinyl peptide molecule in different surroundings, we started from the coordinates of the X-ray crystal structure and performed a detailed conformational search in gase phase, as well as in water and chloroform environment. During the search, only conformations for which the potential energy differed from the most stable conformer within the range of 20 kJ mol$^{-1}$ were kept. The decision to disregard all conformers with higher energies is based on studies of various authors who showed that bioactive conformations lie within this threshold.[34−36] All generated conformers were once more minimized and repeating structures were discarded. Table 2 shows the energies of the most stable conformers found for the various surroundings relative to the energy of the arrangement of a single molecule in the crystal (see computational methods part for details). The XCluster[37] program was used to differentiate between various types of conformers, e.g., to determine how many of the conformers in all three surroundings form the N1H−O4H bond. Clustering of all of the conformers was done with respect to the atoms in the backbone that take part in forming of this bond. Results are also summarized in Table 2.

In contrast to the starting structure taken from the X-ray crystal structure, which is more or less linear, all of the conformers generated in the conformational search in gas phase as well as in chloroform and water surroundings possess bent
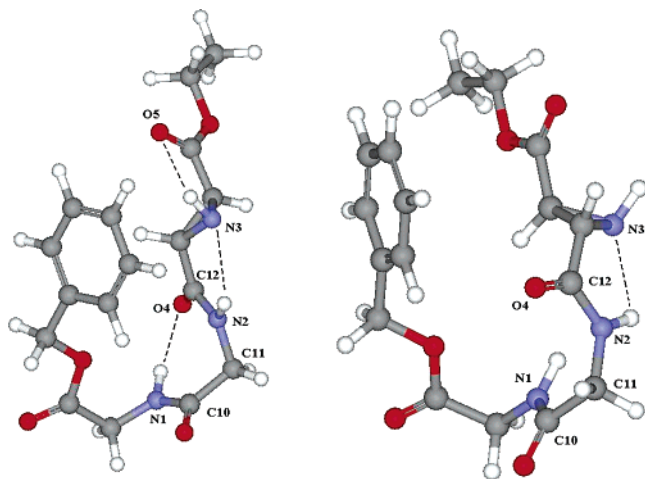
**Figure 7.** Most stable conformers generated in a conformational search in gas phase (left) and water (right). Important intramolecular hydrogen bonds (dotted lines) and the atoms that are involved in their forming are labeled.

structures. Figure 7 shows the most stable conformers in gas phase (left) and in water (right).

The investigations employing the XCluster program show that the reasons for the stability of the bent structures strongly depend on the environment. As expected for the gas-phase, intramolecular hydrogen bonds are the most important ones. The strongest one is located between N1H and O4 atoms (Figure 7). For this bond, the computations predict bond lengths between 1.9 and 2.1 Å. Its importance for the gas phase is underlined by the fact that in about 75% of all studied conformers this bond is formed. Additional hydrogen bonds appear between O1−N1H, N2H−N3, O5−N3H, and O6−N3H centers but are all less important as can be seen from their atomic distances which are computed to be greater than 2.2 Å.

As expected, in more polar solvents, hydrogen bonds as stabilizing factors become less important so that for water as solvent the stabilization of the bent conformers always results from various similar important contributions (various hydrogen bonds, van der Waals interactions). It is interesting to note, that the strengths of the hydrogen bonds are differently influenced by the solvent. The most striking example is the N1H−O4 hydrogen bond. As already discussed, in the gas phase, this bond is formed in 75% of conformers under investigation, and its importance is further underlined by the fact that this bond is found in most of the energetically lower lying conformers, e.g., also in the most stable conformer. For water as solvent only 12 % of the conformers under investigation form this bond and different to the gas phase the bond is only found in the energetically higher lying conformers. For example, in the most stable conformer in water, this hydrogen bond is not formed.

Our analysis shows that for gas phase and medium polar surroundings the intermolecular interactions which stabilize the linear form in the crystal (gas phase 270 kJ mol$^{-1}$, Figure 6) clearly overcompensate the intramolecular interactions which would favor the bent structures (gas phase 82 kJ mol$^{-1}$, Table 2). The considerably stronger interaction in the crystal explains the linear form found in the X-ray diffraction experiment, since remaining intermolecular interactions between the bent molecules and entropy effects which would also favor bent structures are expected to be much smaller. Only in very polar environments the relation flips. Here already the intramolecular interactions within a single molecule in a bent structure (53 kJ mol$^{-1}$, Table 2) are stronger than the intermolecular interaction of a single molecule with all its neighbors for which dimer
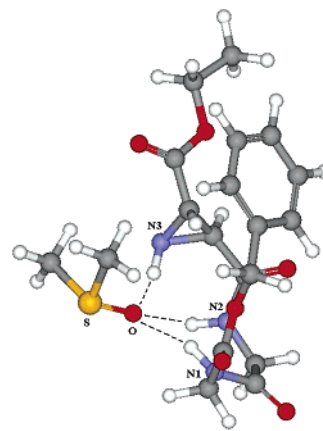


**Figure 8.** Most stable geometry aziridinyl peptide−DMSO complex. Intermolecular H bonds are represented by dashed lines.

calculations predict a value of 42 kJ mol$^{-1}$ (Figure 6). For the medium polar solvent chloroform, our calculations also predict that the sum of the intermolecular forces (126 kJ mol$^{-1}$) leading to a linear conformation predominates the intramolecular interactions (66 kJ mol$^{-1}$) which would favor a bent structure. $^1$H NMR dilution studies in CDCl$_3$ confirm this prediction since at dilution the signals for the all NH protons are shifted significantly to higher field ($\Delta\delta$ = 0.05−0.34 ppm, see Experimental Section) which means that these protons are involved in intermolecular H-bonding. An additional confirmation of the lack of intramolecular H bonds in CHCl$_3$ is provided by NOESY spectra in CDCl$_3$ which only show cross-peaks for the ring protons C13H and C14H with the amide proton N2H as well as for the C11H protons with the N1H amide proton.

Up to now, our calculations treat the environment as a polarizable continuum without any molecular structure, i.e., solvents themselves which can form hydrogen bonds to the solute are not described properly. To investigate how hydrogen bonds between solvent and solute influence the energetics of the system, we surrounded a single molecule with 1−5 molecules of DMSO. The extended conformational analysis and further minimizations predicted only structures with intermolecular H bonds. Even the presence of only one molecule of DMSO was already sufficient to prevent the intramolecular H-bond formation by involving all NH groups of the aziridinyl peptide in intermolecular hydrogen bonds to the oxygen of the DMSO molecule. The most stable geometry of the complex of one DMSO molecule and the aziridinyl peptide is depicted in Figure 8. The binding energy in this complex is already 130 kJ mol$^{-1}$ and increases with the number of DMSO molecules involved to achieve 299 kJ mol$^{-1}$ with five of them surrounding the aziridinyl peptide. Consequently, compared to the binding energies within the crystal structure this predicts a solution of the crystalline aziridinyl peptide in DMSO. It nicely explains the experimental finding that crystals of the compound are only soluble in hot medium polar and polar solvents (water, THF, DMSO, CHCl$_3$).

**Evaluation of the Accuracy of Different Force Fields.** The present study is a first step of a comprehensive investigation about various effects which govern the inhibition properties of aziridine based cysteine protease inhibitor.[38] During the inhibition mechanism, a covalent bond is formed and as indicated in various experimental studies also the proteinic environment cannot be neglected. Therefore, the investigation will mainly be performed with QM/MM Ansätze. To ensure a reliable description of the MM part in the present study, we evaluate the accuracy of different force fields for the description of the
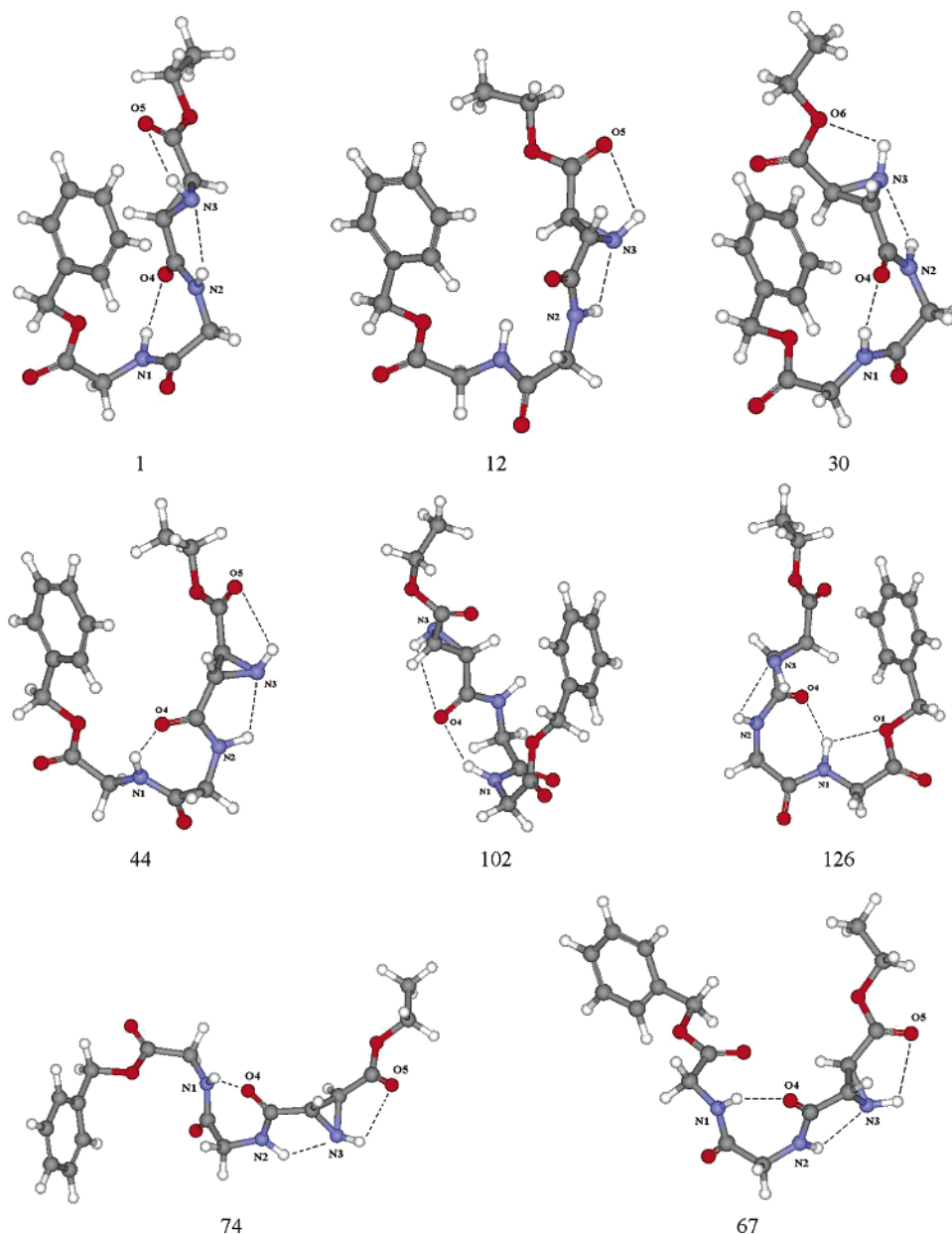
Properties of an Aziridinyl Peptide

*J. Phys. Chem. A, Vol. 108, No. 51, 2004* **11403**



**Figure 9.** Conformers selected to test the accuracy of various force fields. Intramolecular H bonds and the atoms that are involved in their forming are labeled. The conformers are represented by the number of their position in the list of the energetically sorted conformers of the MMFF94 force field.

conformers of aziridinyl peptides by comparing their results with ab initio data.

For this purpose, eight different conformers (118 in total) generated in an extended conformational search in the Macro-Model8.0 suit of programs using MMFF94s[39,40] force field were used. The various conformers are depicted in Figure 9. They are represented by the number of their position in the list of the energetically sorted conformers of the MMFF94 force field. They were picked in such a manner that their energies as well as their geometries differ significantly. In the first step we used the geometries predicted by the MMFF94 force field and performed single point energy calculations with different basis sets and functionals. For these computations, the RIDFT module of the TURBOMOLE[41] program package was used. The relative energies (conformer 1 was assigned zero energy) calculated for each conformer are presented in Table 5. The numbering of the conformers is identical to Figure 9. Table 3 shows that the relative energies computed with different basis sets (standard SV(P), TZVP, and TZVPP) and functionals (B[42]P86,[43] BLYP,[44]

B3[45]LYP, and PBE[46]) vary less than about $3-4$ kJ mol$^{-1}$. Although the differences between different functionals and basis sets seem to be small, Table 3 points to differences between the MMFF94 force field and DFT. One example is conformer 67 which within the MMFF94 computations was found to be about 15 kJ mol$^{-1}$ less stable than conformer 1 (see Table 4). Various DFT approaches predict it to be about $12-14$ kJ mol$^{-1}$ more stable than 1 (see Table 3).

To study such differences in more detail, in a second step, we investigated the relative energies of fully geometry optimized conformers. Since the influence of functionals and basis sets seems to be small, only the TZVP basis set in combination with the BP86 functional was employed to reoptimize the geometries of the conformers under investigation. The resulting relative energies were compared with the predictions of various force fields (MMFF94s, MM3*,[47] AMBER*,[48-50] and OPLS-AA[51]). In addition, we performed MP2/TZVP calculations using the BP86/TZVP geometries. These data are summarized in Table 4.

**11404** *J. Phys. Chem. A, Vol. 108, No. 51, 2004*

Schirmeister et al.

**TABLE 3: Relative Energies of Selected Conformers with Respect to Conformer 1 Computed with Various Basis Sets and Functionals[a]**

| | basis sets[b] | | | functionals[c] | | | |
|---|---|---|---|---|---|---|---|
| conf | SV(P) | TZVP | TZVPP | BP86 | BLYP | B3LYP | PBE |
| 12 | 19 | 23 | 22 | 23 | 22 | 22 | 21 |
| 30 | 19 | 16 | 17 | 16 | 16 | 16 | 16 |
| 44 | 44 | 44 | 45 | 44 | 43 | 44 | 42 |
| 67 | −10 | −12 | −12 | −12 | −14 | −11 | −7 |
| 74 | 0 | −3 | −4 | −3 | −5 | −1 | 4 |
| 102 | 30 | 32 | 31 | 32 | 31 | 30 | 30 |
| 126 | 68 | 66 | 64 | 66 | 64 | 64 | 64 |

[a] The geometrical structures can be taken from Figure 9 (all values are in kJ mol$^{-1}$). [b] BP86 functional was used. [c] TZVP basis set was used.

**TABLE 4: Relative Energies of Selected Conformers (conf) with Respect to Conformer 1 Computed with Various Force Fields, the B86/TZVP and MP2/TZVP Approach[a]**

| | force fields | | | | ab initio | |
|---|---|---|---|---|---|---|
| | | | | | B86/ | MP2/ |
| conf | MMFF94s | MM3* | AMBER* | OPLS-AA | TZVP | TZVP |
| 12 | 5 | −7 | 10 | 5 | 10 | 21 |
| 30 | 9 | 2 | 3 | −3 | 9 | 8 |
| 44 | 13 | −3 | 6 | 7 | 19 | 33 |
| 67 | 15 | 11 | 16 | 0 | −5 | 5 |
| 74 | 16 | 9 | 13 | −3 | 2 | 16 |
| 102 | 19 | −1 | 12 | 5 | 19 | 30 |
| 126 | 20 | 0 | 9 | 18 | 24 | 16 |

[a] The geometrical structures can be taken from Figure 9 (all values are in kJ mol$^{-1}$).

The MMFF94s force field showed good accordance to RIDFT calculations for all conformers except conformers 67 and 74 for which already Table 3 showed the strongest deviations. Comparing the relative energy predicted by the BP86/TZVP approach for conformer 67 at the MMFF94 geometry (−12 kJ mol$^{-1}$, see Table 3) with its relative energy computed at geometry optimized for DFT (−5 kJ mol$^{-1}$, see Table 3) and with the MMFF94 value (+15 kJ mol$^{-1}$, see Table 4), it is seen that the difference results only partially from differences in the geometries. In this respect, it is interesting to note that the MP2 predictions (+5 kJ mol$^{-1}$, see Table 4) are closer to the MMFF94s results than the DFT approach. This behavior could stem from van der Waals interactions which are not appropriately described by some DFT functionals. This explanation is supported by the relative energy predicted by the PBE functional which for conformer 67 is in better agreement with the MP2 result than other functionals (see Table 3). Taking the differences between DFT and MP2 into account both MMFF94 and AMBER are found to describe the relative energies of the various conformers quite accurately. The other force fields seem to be less appropriate.

**Raman Spectroscopy.** A detailed vibrational analysis of the aziridine containing peptide (**2**) and its building block (**1**) has been performed in order to investigate the hydrogen bonding pattern. The FT-Raman spectra of neat **1** and **2** have been recorded and the vibrational assignment of the bands was achieved with the help of theoretical calculations as well as the investigation of the deuterated compounds. The vibrational wavenumbers and Raman scattering activities have been calculated subsequently to the optimization of the molecular structure within the Gaussian98[52] program. Several functionals (BPW91, B3LYP, and B3PW91) and different basis sets (6-31+G(d) and 6-311++G(d,p)) have been applied for **1** to calculate the vibrational wavenumbers. Since the best agreement
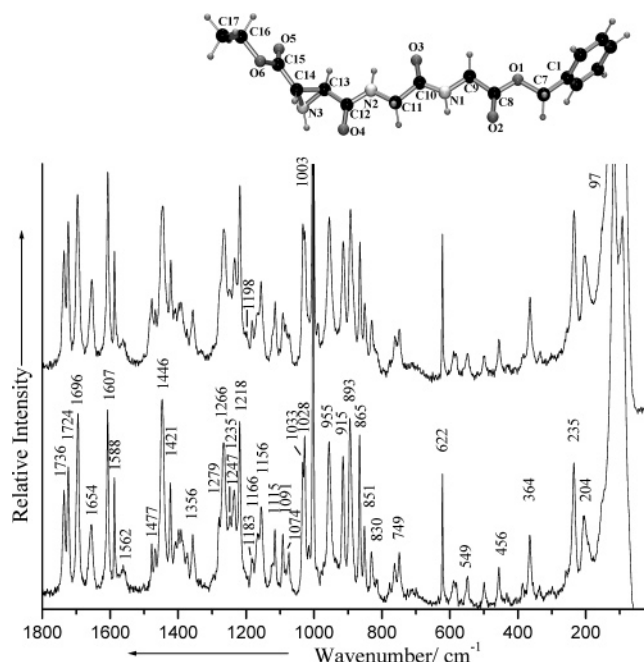


**Figure 10.** FT-Raman spectrum of (**2**) (bottom) in comparison with the FT-Raman spectrum of the deuterated form (**D2**) (top).

between the calculated and experimental wavenumbers has been obtained with the BPW91 functional, the latter combined with the 6-311G(d,p) has been used in the calculations of **2**. The calculated vibrational modes have been visualized with the HyperChem[53] program. Moreover, the potential energy distribution (PED) for each normal mode has been calculated,[54] which allowed a better understanding of the contribution of the displacement coordinates to the normal modes in terms of internal coordinates.

The vibrational analysis of the electrophilic building block (**1**) and of the deuterated form (**D1**) is included in the Supporting Information.

Figure 10 depicts the FT-Raman spectrum of **2** in comparison with the spectrum of the deuterated form (**D2**) between 0 and 1800 cm$^{-1}$ (the wavenumber region between 1800 and 3600 cm$^{-1}$ can be found in the supporting material see Figure C).

Unfortunately, the NH hydrogen atoms could not be replaced completely by the deuterium isotope. Nevertheless, the ND stretching modes can be clearly recognized at lower wavenumbers. The NH aziridine stretching has been assigned in analogy to **1** to the band at 3264 cm$^{-1}$ and is shifted to 2430 cm$^{-1}$ in the spectrum of the deuterated species. Two amide NH stretching modes arise at higher wavenumbers (3344 and 3317 cm$^{-1}$, respectively). This mode arises at 3288 cm$^{-1}$ in α-gly-cylglycine[56] and at 3277 cm$^{-1}$ in its hydrochloride,[56] whereas in Poly(Gly), the amide NH stretching mode arise[20a] at 3301 cm$^{-1}$. Hence, the hydrogen bonding of the aziridine peptide amides is significantly weaker than the hydrogen bonding of the polypeptide. Nevertheless, concerning the bonding interaction of the aziridine NH, this is stronger than in the electrophilic building block (**1**) since it arises at about 19 cm$^{-1}$ lower wavenumbers. In the region of skeletal vibrations, however, only changes in intensity can be observed upon deuteration. A detailed vibrational analysis of **2** is given in Table 5 (for a vibrational assignment of the modes in the wavenumber region 1800−3600 cm$^{-1}$ see supporting material table B).

In the case of **2**, the carbonyl stretching vibrations are well differentiated, and 4 bands can be observed in the FT-Raman spectrum (see Figure 10) of this derivative corresponding to its

Properties of an Aziridinyl Peptide

*J. Phys. Chem. A, Vol. 108, No. 51, 2004* **11405**

**TABLE 5: Experimental and Calculated Vibrational Wavenumbers (in cm$^{-1}$) of 2 and Their Vibrational Assignment (1800−800 cm$^{-1}$ Wavenumber Region + N−H Stretch Vibrations)$^a$**

| observed | BPW91/11G(d,p) | vibrational assignment, (PED %) |
|---|---|---|
| 3344 | 3486 | $\nu$N1−H(99) (for $\nu$N1-D **2484**) |
| 3317 | 3461 | $\nu$N2−H(99) (for $\nu$N2-D **2454**) |
| 3264 | 3331 | $\nu$N3−H(100) (for $\nu$N3-D **2430**) |
| 1736 | 1751 | $\nu$C15=O5(75) + $\nu$14-C15(6) |
| 1724 | 1738 | $\nu$C8=O2(77) + $\nu$O1−C8(6) |
| 1696 | 1703 | $\nu$C10=O3(64) + $\nu$N1−C10(10) + $\nu$C12=O4(7) |
| 1654 | 1677 | $\nu$C12=O4(64) + $\nu$C12−N2(11) + $\nu$C10=O3(8) |
| 1607 | 1607 | $\nu$Phenyl(58)(e$_{2g}$$^a$) + $\delta^{in}$PhenylH(12) + $\delta^{in}$Phenyl(7) |
| 1588 | 1587 | $\nu$Phenyl(70)(e$_{2g}$$^b$) + $\delta^{in}$PhenylH(9) + $\delta^{in}$Phenyl(7) |
| 1562 | 1501 | $\nu^{as}$C10−N1−C9(39) + $\nu$C11−C10(7) + $\nu$N2−C12(6) + $\delta^{in}$CN1−H(24) + $\delta^{in}$CN2H(5) |
|  | 1489 | $\nu$Phenyl(37)(e$_{1u}$$^a$) + $\nu$C1−C7(7) + $\delta^{in}$PhenylH(56) |
| 1477 | 1485 | $\nu$N2−C12(31) + $\nu$C11−N2(10) + $\nu$N1−C10(8) + $\delta^{in}$CN2−H(22) + $\nu$C12−C13(7) |
| 1468 | 1476 | $\delta^{scis}$C16H$_2$(54) + $\delta^{as}$CH$_3$(34) |
|  | 1459 | $\delta^{scis}$C7H$_2$(93) |
| 1447br | 1458 | $\delta^{as}$CH$_3$(73) + $\delta^{scis}$C16H$_2$(10) |
|  | 1454 | $\delta^{scis}$C11H$_2$(84) |
|  | 1446 | $\nu$Phenyl(26)(e$_{1u}$$^b$) + $\delta^{in}$PhenylH(45) |
|  | 1445 | $\delta^{as}$CH$_3$(90) |
| 1423 | 1445 | $\delta^{scis}$C9H$_2$(83) |
| 1407 | 1413 | $\nu^{as}$C15−C14−C13(30) + $\nu^{s}$C14−N3−C13(12)+ $\delta$CC14−H(25) |
| 1399 | 1378 | $\delta^{s}$CH$_3$(58) + $\delta^{wag}$C16H$_2$(12) +$\nu$C16−C17(12) |
| 1392 | 1367 | $\delta^{wag}$C7H$_2$(48) + $\nu$C9−C8(11) + $\nu$C8−O1(6) + $\nu$C7−C1(6) |
| 1373 | 1349 | $\delta^{wag}$C16H$_2$(47) + $\delta^{s}$CH$_3$(21) |
| 1356 | 1346 | $\nu$Phenyl(84)(b$_{2u}$) |
|  | 1338 | $\delta^{wag}$CH$_2$(amide, Bn)+ $\nu$C11−C10(6) |
|  | 1322 | $\delta^{wag}$C9H$_2$(20$^+$) + $\delta$CC13−H(14) + $\nu$C9−C8(5) |
|  | 1316 | $\delta^{in}$PhenylH(81)(a$_{2g}$) |
| 1279sh | 1291 | $\delta^{wag}$C11H$_2$(33) + $\delta$CC13−H(12) |
| 1266 | 1261 | $\nu$azi(30)(breathing) + $\delta$CN3−H(22) + $\delta$CC14−H(12) |
| 1247 | 1256 | $\delta^{twist}$C16H$_2$(92) + $\delta^{rock}$CH$_3$(6) |
| 1235 | 1212 | $\delta$CN1−H(21) + $\nu$C8−O1(10) + $\nu$C10−N1−C9(13) + $\delta^{twist}$C7H$_2$(13) |
| 1218 | 1209 | $\nu$C7−C1(39) + $\delta^{in}$PhenylH(11) + $\nu$Phenyl(6) |
|  | 1208 | $\delta^{twist}$C7H$_2$(74) |
|  | 1203 | $\delta$CN3−H(44), $\delta$CC14−H(14)$^{scis}$ + $\nu$C15−O6(7) + $\delta$C13C14−C15(9) |
| 1183 | 1196 | $\delta^{twist}$C11H$_2$(71) + $\delta$CN2−H(8) + $\nu$N2−C11(7) |
|  | 1191 | $\delta^{twist}$C11H$_2$(33) + $\delta^{twist}$C9H$_2$(16) + $\delta$CN2−H(14) + $\nu$N2−C11(7) |
|  | 1189 | $\delta^{twist}$C9H$_2$(79) |
| 1166 | 1178 | $\nu$O1−C8(22) + $\delta^{twist}$C9H$_2$(33) + $\delta$CN1−H(10) |
|  | 1171 | $\delta$PhenylH(59)(e$_{2g}$$^a$) + $\nu$O1−C8(8) |
| 1156 | 1157 | $\delta$PhenylH(81)(b$_{2u}$) + $\nu$Phenyl(11) |
|  | 1142 | $\nu$C15−O6(25) + $\delta^{rock}$C16H$_2$(15) + $\delta^{rock}$CH$_3$(7) + $\delta$CC14−H(5) + $\nu$C11−N2(5) |
|  | 1139 | $\delta^{rock}$C16H$_2$(46) + $\delta^{rock}$CH$_3$(18) + $\nu$C15−O6(8) |
| 1126sh | 1134 | $\delta$CC14−H(24), $\delta$CN3−H(8)$^{twist}$ + $\nu$C15−O6(10) + $\nu$N2−C11(8) + $\nu$N1−C9(6) + $\nu$C14−C15(6) |
| 1115 | 1120 | $\delta$CC13−H(21), $\delta$CN3−H(9)$^{wag}$ + $\nu$N1−C9(18) + $\nu^{s}$C12−N2−C11(13) |
| 1091 | 1104 | $\nu$C16−C17(28) + $\delta^{rock}$CH$_3$(44) |
| 1084 | 1085 | $\nu$Phenyl(42)(e$_{1u}$$^b$) + $\delta$PhenylH(36)(e$_{1u}$$^b$) |
| 1074 | 1077 | $\nu$N2−C11(26) + $\nu$N1−C9(22) + $\nu$C10−N1(6) |
| 1074 | 1074 | $\delta$CC13−H(51), $\delta$CC14−H(10)$^{wag}$ |
| 1033 | 1028 | $\nu$Phenyl(55)(e$_{1u}$$^a$) + $\delta$PhenylH(17)(e$_{1u}$$^a$) |
| 1028 | 1018 | $\nu^{as}$C17−C16−O6(58) + $\delta^{rock}$CH$_3$(8) + $\delta$CC14−H(6) |
| 1016 | 1009 | $\delta$CC13−H(23), $\delta$CC14−H(18), $\delta$CN1−H(9) + $\delta$CC−C12(10) |
| 1003 | 991 | $\nu$Phenyl(86)(trig breathing) |
|  | 981 | $\delta^{rock}$C11H$_2$(20) + $\delta^{rock}$C9H$_2$(11) + $\nu$C13−C12(6) |
|  | 978 | $\delta^{rock}$C9H$_2$(40) + $\delta^{out}$OC=O2(7) |
|  | 972 | $\delta^{out}$PhenylH(69) |
|  | 971 | $\delta^{rock}$C11H$_2$(15) + $\delta^{rock}$C9H$_2$(10) + $\nu$C9−C8(6) + $\delta^{out}$OC=O3(6) |
| 955 | 962 | $\nu$C13−C12(9) + $\delta^{rock}$C11H$_2$(19) + $\delta^{out}$OC=O3(7) |
|  | 946 | $\delta^{out}$PhenylH(81) |
|  | 944 | $\delta^{rock}$C7H$_2$(64) |
|  | 932 | $\nu$C14−C15(12) + $\nu$N3−C13(7) + $\nu$C11−C10(5) + $\delta^{out}$PhenylC(5) |
|  | 923 | $\delta^{out}$PhenylC(15) + $\delta^{out}$PhenylH(14) + $\nu$O1−C7(7) + $\nu$C14−C15(7) |
| 915 | 915 | $\nu$O1−C7(29) + $\nu$C9−C8(8) + $\nu$C11−C10(7) |
| 893 | 885 | $\nu$O1−C7(29) + $\delta^{out}$PhenylH(53) |
| 865 | 873 | $\nu$N3−C13(26) + $\delta$CC−C12(7) + $\delta^{rock}$CH$_3$(6) |
| 851 | 861 | $\nu$N3−C14(36) + $\nu$C13−C14(18) + $\delta$CC−C15(18) + $\delta^{out}$OC=O5(7) |
| 830 | 843 | $\nu$O6−C16(33) + $\nu$N3−C13(16) + $\delta^{rock}$CH$_3$(16) |
| 817 | 828 | $\delta^{out}$PhenylH(100) |
| 814 | 816 | $\nu$C7−C1(21) + $\nu$C9−C8(9) + $\nu$Phenyl(16) + $\delta$Phenyl(7) |
| 778 | 790 | $\delta$rockCH3(30) + $\delta$rockC16H2(55) |
| 763 | 756 | $\delta$outCC−C12(41) + $\delta$outOC=O4(14) |

**TABLE 5 (Continued)**

| observed | BPW91/11G(d,p) | vibrational assignment, (PED %) |
|---|---|---|
| 749 | 747 | δoutPhenyl(31) + δoutPhenylC(27) + δoutPhenylH(23) |
| | 713 | δoutCC−C12(14) + δoutOC=O5(11), δoutOC=O4(9)in-phase |
| | 697 | δoutCC−C15(21) + δoutCC−C4(12) + δoutOC=O4(7) |
| | 691 | δoutPhenyl(47) + δoutPhenylH(24) + δoutPhenylC(12) |
| | 674 | δCC−C12(15) + δCC−C15(17) |
| | 637 | δinamide(46) |
| 622 | 618 | δinPhenyl(86) |
| 590 | 604 | δoutCN1−H(15) + δoutOC=O3(11) + δrockC11H2(24) |
| | 569 | δoutPhenylC(10) + δPhenyl(9) + δoutOC=O2 |
| | 565 | δoutOC=O2(11) + δtwistC9H2(22) + δoutO1C8C9(15) |
| | 562 | δoutCN2−H(33) + δoutCCC12(15) + δoutC12N2C11(8) |
| 549 | 547 | δinN2C11C10(=O3)N1(28) + δPhenyl(9) |
| 499 | 497 | δoutPhenylC(31) + δPhenyl(14) + δinN2C11C10(5) |
| 456 | 433 | δinC16O6C15=O5(31) + δCC−C12(10) |
| | 401 | δinC16O6C15=O5(23) + δoutPhenylC(8) + δoutPhenyl(9) |
| 386 | 398 | δoutPhenyl(86) |
| 364 | 354 | δout(O=)C15C14C13C12(=O)N2(73) |
| | 246 | δC15CC−C12(36) + δinOC=O5(13) |
| 235 | 221 | δC15CC−C12(34) |
| 204 | 204 | δoutC12N2C11C10(30) |

[a] The calculations were done at the BPW91/6-311G(d,p) level. The calculated PED values are given in parentheses for each mode.

4 carbonyl groups. The carboxylate moieties give rise to the bands at higher wavenumbers, namely, the ethyl ester at 1736 cm$^{-1}$ and the benzyl ester at 1724 cm$^{-1}$. The later slightly couples to the adjacent amide carbonyl. However, the relative low wavenumbers at which the ester carbonyl bands arise tend toward a notable hydrogen bonding. The corresponding band in the spectrum of **1** arises at 1737 cm$^{-1}$.

Due to the electron delocalization in the amide backbone, the amide carbonyl bands are shifted usually to lower wavenumbers. The band at 1696 cm$^{-1}$ corresponds to the C10=O3 stretch vibration, whereas the band at 1654 cm$^{-1}$ corresponds to the carbonyl moiety (C12=O4) adjacent to the aziridine ring. The DFT computed wavenumbers (see Table 5) of the optimized molecular structure of **2** (see Figure D in the Supporting Information) are in good agreement with the experimental data. Nevertheless, the band at 1654 cm$^{-1}$ is predicted at higher wavenumbers with about 20 cm$^{-1}$, whereas the other carbonyl modes are calculated with a better accuracy. Therefore, the Raman spectrum of the solid shows probably stronger hydrogen bonding interaction involving this group than it is predicted by the gas-phase optimization. Nonetheless, the crystal structure analysis shows stronger H-bonding interaction for the O4c (see Table 1), the amide carbonyl adjacent to the aziridine ring, which is in agreement with the experimental Raman data. Moreover, this C=O bond is the longest carbonyl bond in the solid-state structure and in the gas-phase calculations by the DFT methods. Compared with the IR and Raman spectra of α-glycylglycine or its hydrochloride[56] or the more recent near-resonance Raman study[20f] on single-crystal glycylglycine·1.5H$_2$O, where, however, the dipeptide appears as a zwitterion, the same conclusions can be drawn. The amide I bands[20] appear in the IR spectrum of the dipeptide[56] at 1674 and 1661 cm$^{-1}$, but at 1663 and 1622 cm$^{-1}$ in the Raman spectrum of the single crystal[20f] reflecting the much shorter intermolecular O···H bonds (in the range of 1.900 to 2.128 Å) compared with (**2**). Sieler et al.[19,20d] also reported Raman spectra of the single-crystal glycylglycine and in solution. The amide bands (at 1665 and 1624 cm$^{-1}$) in the solid-state spectrum[19] are consistent with the data of Pajnici et al.[20f] Nonetheless, these modes shift to considerably higher wavenumbers in the case of the solvated molecule[19,20d] giving rise to two bands at 1675 and 1692 cm$^{-1}$. Sieler et al.[19,20d] showed that the amide I doublet arises from vibrational mixing with water molecules and ruled out the possibility that the amide

I subbands result from peptides with different hydrogen bonding between their CO groups and adjacent water molecules. Poly-(L-Gly) shows one amide I band at 1674 cm$^{-1}$ in the Raman spectrum, but two bands appear[20a] in the IR spectrum at 1685 and 1636 cm$^{-1}$. Nevertheless, in the case of **2**, the significant splitting of the amide I band is due to the presence of the two differently H-bonded carbonyl moieties as shown also by the solid-state structure. Hence, one carbonyl group is weakly H-bonded, whereas the carbonyl group adjacent to the aziridine ring is involved in both intermolecular H-bonding with the amide NH of a neighboring molecule and intramolecular interactions with the aziridine NH. As shown by the X-ray structure analysis, the later group is involved also in intermolecular interaction with the benzyl ester carbonyl and therefore the aziridine NH stretch of **2** is more strongly involved in H-bonding than in **1** arising at lower wavenumbers.

Although the DFT optimized structure (see Figure D in the Supporting Information), where the optimization started from the crystal structure coordinates of **2**, led to a different conformer, the calculated wavenumbers are in good agreement with the experimental data and the PED information corresponds to the experimental data of the investigated analogue compounds and to those from the literature.[19,20,56] The agreement between the calculated and the observed wavenumbers is due probably to the fact that the calculated bond lengths for the gas-phase structure are in very good agreement with the crystal structure, even though the bond angles present striking discrepanicies (see Figure D in the Supporting Information).

In the following, the backbone vibrations of **2** will be briefly discussed (see Table 5). The amide II band has usually very low intensity in the Raman spectra if recorded with visible excitation. The FT-Raman spectra of **2** present a shoulder at 1562 cm$^{-1}$ which could be assigned to this mode. Nevertheless, the calculations predicted two modes corresponding mainly to the CN stretch combined with NH bending mode at 1501 and 1485 cm$^{-1}$. In the Raman spectrum the band of weak intensity at 1477 cm$^{-1}$ is most likely to correspond also to an amide II band involving predominantly the N2 atom. This mode arises usually around 1570 cm$^{-1}$ in model peptides of trans configuration, but around 1475 cm$^{-1}$ in cis configuration,[57] whereas for Poly(L-Gly),[20a] two bands at 1564 and 1515 cm$^{-1}$ can be observed. The amide III band of **2** presents medium intensity

Properties of an Aziridinyl Peptide

*J. Phys. Chem. A, Vol. 108, No. 51, 2004* **11407**

in the FT-Raman spectrum at 1235 cm$^{-1}$ and corresponds well with the assignment of Poly(L-Gly).[20a] The polypeptide presents two amide III bands at 1233 and 1220 cm$^{-1}$, respectively. The second amide III vibration of **2** could be assigned based on the DFT calculations to the band at 1183 cm$^{-1}$, but however, the contribution of the CH$_2$ twist vibration for this mode is high. In contrast, the aziridine ring stretching which also involves CN stretch and NH bending arise at much lower wavenumbers, namely, at 1266 cm$^{-1}$ for the ring breathing mode and in the case of the dominant CN stretching modes at 865 and 851 cm$^{-1}$. Very often these modes are assigned as ring deformations,[55,58] but the PED calculations and the atomic displacements showed that a stretching assignment is more proper in terms of internal coordinates. Moreover, an $n$-membered ring presents $3n - 6$ degrees of freedom[59] which are described as $n$ stretching modes and $2n - 6$ symmetrized bending and torsion modes. In the case of a three-membered ring, this leads to 3 degrees of freedom corresponding to 3 possible stretching modes.

Several modes corresponding to C−O, N−CH$_2$, and C−C stretching vibrations arise in the 1400−800 cm$^{-1}$ spectral region. The ester C−O bond is involved into vibrational modes at comparably higher wavenumbers (1166, 1156, and 1126 cm$^{-1}$) than the O-Et or O−Bn (1028, 915, 893, and 830 cm$^{-1}$) due to its partial double bond character. The N−CH$_2$ stretching gives rise to bands at significantly lower wavenumbers (1126, 1115, and 1074 cm$^{-1}$) than the amide II or III modes.

The amide deformation modes have low intensity in the Raman spectrum in the 800−250 cm$^{-1}$ spectral region, but very strong modes can be observed around 100 cm$^{-1}$ where out-of-plane deformation modes probably overlap with lattice vibrations of the crystal unit. Nevertheless, the calculated Raman intensities of the latter modes are very strong.

Finally, we skip a detailed discussion of the CH$_2$ and CH$_3$ bending modes (see Table 5), but it is worth noting that the strong band at 1446 cm$^{-1}$ corresponds mainly to the asymmetrical bending of the CH$_3$ group, since it can be observed in the Raman spectra of **2** and **1,** but not in analogue compounds without the methyl group.

## Conclusions

The X-ray structure analysis in combination with the computations of various bond strength clearly shows that the intermolecular hydrogen bonding network established in the solid state is responsible for the zigzag arrangement of the aziridinyl peptide (**2**).

Conformational analysis of a single molecule in different environments which were taken into account by the continuum Ansatz showed that a single aziridinyl peptide molecule possesses a bent structure. Various intramolecular interactions are found to be responsible, but for the gas phase and for medium polar solvents, the N1H−O4 hydrogen bond plays a prominent role. For more polar solvents, several interactions become similarly important since especially the N1H−O4 hydrogen bond is considerably weakened. As indicated by computations, the linear form found in the X-ray experiment results due to stabilization by strong intermolecular interactions which overcompensate the intramolecular ones. Even for medium polar solvents such as CHCl$_3$, the intermolecular forces are predicted to be stronger than the intramolecular ones. This is confirmed by NMR studies. Only for strong polar solvents such as water, the order of inter- and intramolecular interactions flips.

If DMSO as a solvent is employed the intermolecular bonds between DMSO and the aziridinyl peptide replace the intramolecular ones leading to a widened conformation.

A detailed vibrational analysis of the title compound has also been performed. The Raman spectra show stronger H-bonding of the aziridine NH unit in the solid state of **2** than in the electrophilic building block (**1**). The electrophilic building block probably presents only intramolecular interactions, whereas the aziridine NH of the peptide derivative is also involved in moderately strong intermolecular H-bonding.

Our analysis indicates that **2** and the related epoxide loxistatin behave quite similar although they possess different peptide residues. Both show a more or less linear conformation and as indicated by our computations for **2** do not build up intramolecular H bonds in DMSO and CHCl$_3$. The main difference between both inhibitors, namely, the participation of the aziridine-NH group in an intermolecular bonding network, seems to be less important in polar solutions. However, it could lead to a stronger stabilization of **2** in crystalline state. Since the intermolecular H bonds involving the peptide bonds seem to be most important, we predict that **2** and related compounds in its complexes with the target cysteine protease papain will adopt a similar structure like loxistatin or related epoxysuccinyl peptides.

**Supporting Information Available:** Anisotropic displacement parameters (ADP) drawn at the 50% probability level and a detailed description of the synthesis and the analytical data for the electrophilic building block. Molecular structure, crystallographic tables, and full bond lengths and angles for **2**. Vibrational analysis of the electrophilic building block (**1**) and of the deuterated form (**D1**). This material is available free of charge via the Internet at http://pubs.acs.org.

## References and Notes

(1) Otto, H.-H.; Schirmeister, T. *Chem. Rev.* **1997**, *97*, 133−171.
(2) Schirmeister, T.; Klockow, A. *Mini Rev. Med. Chem.* **2003**, *3*, 585−596.
(3) Powers, J. C.; Asgian, J. L.; Ekici, Ö. D.; James, K. E. *Chem. Rev.* **2002**, *102*, 4639−4750.
(4) Albeck, A.; Kliper, S. *Biochem. J.* **2000**, *346 Pt 1*, 71−6.
(5) Eilon, G. F.; Gu, J.; Slater, L. M.; Hara, K.; Jacobs, J. W. *Cancer Chemother. Pharmacol.* **2000**, *45*, 183−91.
(6) Gour-Salin, B. J.; Lachance, P.; Plouffe, C.; Storer, A. C.; Menard, R. *J. Med. Chem.* **1993**, *36*, 720−5.
(7) Matsumoto, K.; Mizoue, K.; Kitamura, K.; Tse, W. C.; Huber, C. P.; Ishida, T. *Biopolymers.* **1999**, *51*, 99−107.
(8) Meara, J. P.; Rich, D. H. *J. Med. Chem.* **1996**, *39*, 3357−66.
(9) Schirmeister, T. *Arch. Pharm. Pharm. Med. Chem.* **1996**, *329*, 239−244.
(10) Schirmeister, T. *Peptide Sci. Present Future* **1998**, 654−656.
(11) Schirmeister, T. *J. Med. Chem.* **1999**, *42*, 560−72.
(12) Schirmeister, T.; Peric, M. *Bioorg. Med. Chem.* **2000**, *8*, 1281−91.
(13) Martichonok, V.; Plouffe, C.; Storer, A. C.; Menard, R.; Jones, J. B. *J. Med. Chem.* **1995**, *38*, 3078−85.
(14) Moroder, L.; Musiol, H. J.; Scharf, R.; Morodor, L. *FEBS Lett.* **1992**, *299*, 51−3.
(15) X-ray analyses of aziridine-2-carboxylates *N*-acylated with amino acids are described in Shao, H.; Jiang, X.; Gantzel, P.; Goodman, M. *Chem. Biol.* **1994**, *1*, 231−234.
(16) Ishida, T.; Sakaguchi, M.; Yamamoto, D.; Inoue, M.; Kitamura, K.; Hanada, K.; Sadatome, T. *J. Chem. Soc., Perkin Trans. 2* **1988**, 851.

(17) (a) Varughese, K. I.; Su, Y.; Cromwell, D.; Hasnain, S.; Xuong, N. H. *Biochemistry* **1992**, *31*, 5172−5176. (b) Katerelos, N. A.; Taylor, M. A.; Scott, M.; Goodenough, P. W.; Pickersgill, P. W. *FEBS Lett.* **1996**, *392*, 35−39. (c) Bhattacharya, S.; Ghosh, S.; Chakraborty, S.; Bera, A. K.; Mukhopadhayay, B. P.; Dey, I.; Banerjee, A. *BMC Struct. Biol.* **2001** *1*, 4. (d) Yamamoto, A.; Tomoo, K.; Matsugi, K.; Hara, T.; In, Y.; Murata, M.; Kitamura, K.; Ishida, T. *Biochim. Biophys. Acta* **2002**, *1597*, 244−251. (e) Zhao, B.; Janson, C. A.; Amegadzie, B. Y.; D'Alessio, K.; Griffin, C.; Hanning, C. R.; Jones, C.; Kurdyla, J.; McQueney, M.; Qiu, X.; Smith, W. W.; Abdel-Meguid, S. S. *Nat. Struct. Biol.* **1997**, *4*, 109−111. (f) Yamamoto, D.; Matsumoto, K.; Ohishi, H.; Ishida, T.; Inoue, M.; Kitamura, K.; Mizuno, H. *J. Biol. Chem.* **1991**, *266*, 14771−14777. (g) Kim, M. J.; Yamamoto, D.; Matsumoto, K.; Inoue, M.; Ishida, T.; Mizuno, H.; Sumiya, S.; Kitamura, K. *Biochem. J.* **1992**, *287*, 797−803. (h) Fujishima, A.; Imai, Y.; Nomura, T.; Fujisawa, Y.; Yamamoto, Y.; Sugawara, T. *FEBS Lett.* **1997**, *407*, 47−50. (i) Matsumoto, K.; Murata, M.; Sumiya, S.; Mizoue, K.; Kitamura, K.; Ishida, T. *Biochim. Biophys. Acta* **1998**, *1383*, 93−100.

(18) Mohamadi, F.; Richards, N. G. J.; Guida, W. C.; Liskamp, R.; Lipton, M.; Caufield, C.; Chang, G.; Hendrickson, T.; Still, W. C. *J. Comput. Chem.* **1990**, *11*, 440−467.

(19) Sieler, G.; Schweitzer-Stenner, R.; Holtz, J. S. W.; Pajcini, V.; Asher, S. A. *J. Phys. Chem. B* **1999**, *103*, 372−384.

(20) (a) Tu, A. T. In *Raman Spectroscopy in Biology: Principles and Applications*; John Wiley & Sons: New York, 1982; pp 65−116. (b) Schweitzer-Stenner, R. *J. Raman Spectrosc.* **2001**, *32*, 711−732. (c) Herrebout, W.; Clou, K.; Desseyn, H. O.; Blaton, N. *Spectrochim. Acta A* **2003**, *59*, 47−59. (d) Sieler, G.; Schweitzer-Stenner, R. *J. Am. Chem*. Soc, **1997**, *119*, 1720−1726. (e) Holtz, J. S. W.; Li, P.; Asher, S. A. *J. Am. Chem. Soc.* **1999**, *121*, 3762−3766. (f) Pajcini, V.; Chen, X. G.; Bormett, R. W.; Geib, S. J.; Li, P.; Asher, S. A.; Lidiak, E. G. *J. Am. Chem. Soc.* **1996**, *118*, 9716−9726.

(21) Breuning, A.; Vicik, R.; Schirmeister, T. *Tetrahedron: Asymmetry* **2003**, *14*, 3301−3312.

(22) (a) Kottke, T.; Stalke, D. *J. Appl. Crystallogr.* **1993**, *26*, 615. (b) Kottke, T.; Lagow, R. J.; Stalke, D. *J. Appl. Crystallogr.* **1996**, *29*, 465. (c) Stalke, D. *Chem. Soc. Rev.* **1998**, *27*, 171.

(23) Bruker, SMART-NT, Data Collection Software, version 5.6; Bruker Analytical X-ray Instruments Inc.: Madison, WI, 2000.

(24) Bruker, SAINT-NT, Data Reduction Software, version 6; Bruker Analytical X-ray Instruments Inc.: Madison, WI, 1999.

(25) Sheldrick, G. M. SADABS 2. 05, Empirical Absorption Correction Program; University of Göttingen: Göttingen, Germany, 2001.

(26) Bruker, SHELX-TL, version 6; Bruker Analytical X-ray Instruments Inc.: Madison, WI, 2000.

(27) (a) Flack, H. D. *Acta Crystallogr.* **1983**, *A39*, 876. (b) Bernadinelli, G.; Flack, H. D. *Acta Crystallogr.* **1985**, *A41*, 500.

(28) Ponder, J. W.; Richarde, F. M. An Efficient Newton-like Method for Molecular Mechanics Energy Minimization of Large Molecules. *J. Comput. Chem.* **1987**, *8*, 1016−1024.

(29) Still, W. C.; Tempczyk, A.; Hawley, R. C.; Hendrickson, T. *J. Am. Chem. Soc.* **1990**, *112*, 6127−6129.

(30) Chang, G.; Guida, W. C.; Still, W. C. *J. Am. Chem. Soc.* **1989**, *111*, 4379−4386.

(31) Kolossvary, I.; Guida, W. C. *J. Am. Chem. Soc.* **1996**, *118*, 5011−5019.

(32) (a) Desiraju, G. R. *Angew. Chem.* **1995**, *107*, 2541; *Angew. Chem., Int. Ed. Engl.* **1995**, *34*, 2328. (b) Desiraju, G. R.; Steiner, T. *The Weak Hydrogen Bond in Structural Chemistry and Biology*; Oxford University Press: Oxford, U.K., 1999. (c) Steiner, T. *Angew. Chem.* **2002**, *114*, 50; *Angew. Chem.*, *Int. Ed.* **2002**, *41*, 48.

(33) Jeffrey, G. A. *An Introduction to Hydrogen Bonding*; Oxford University Press: Oxford, U.K., 1997.

(34) Boström, J.; Norrby, P. O.; Liljefors, T. *J. Comput.-Aided Mol. Des.*, **1998**, 12, 383−396.

(35) Siebel, G. L.; Kollman, P. A.; In *Comprehensive Medicinal Chemistry*; Hansch, C., Sammes, P. G., Taylor, B., Ramsden, C. A., Eds.; Pergamon: Oxford, U.K., 1990; Vol. 4, pp 125−138.

(36) Liljefors, T.; Pettrrsson, I.; In *A Textbook of Drug Design and Development*, 2nd ed.; Krosgaard-Larsen, P., Liljefors, T., Madsen, U., Eds.; Overseas Publishers Association: Amsterdam, The Netherlands, 1996; pp 60−93.

(37) Shenkin, P. S.; McDonald. D. Q. *J. Comput. Chem.* **1994**, *15*, 899−916.

(38) Helten, H.; Schirmeister, T.; Engels, B. *J. Phys. Chem.* **2004**, accepted.

(39) Halgren, T. A. *J. Comput. Chem.* **1996**, *17*, 490−512, 520−552, 553−586, 587−615, 616−641.

(40) Halgren, T. A. *J. Comput. Chem.* **1999**, *20*, 720−729, 730−748.

(41) Ahlrichs, R.; Bär, M.; Baron, H.-P.; Bauernschmitt, R.; Böcker, S.; Ehrig, M.; Eichkorn, K.; Elliott, S.; Furche, F.; Haase, F.; Häser, M.; Horn, H.; Huber, C.; Huniar, U.; Kattaneck, M.; Kölmel, C.; Kollwitz, M.; May, K.; Ochsenfeld, C.; Öhm, H.; Schäfer, A.; Schneider, U.; Treutler, O.; Arnim, M. v.; Weigend, F.; Weis, P.; Weiss, H. TURBOMOLE, version 5.6; University of Karlsruhe: Germany, 1988.

(42) Becke, A. D. *Phys. Rev. B* **1988**, *38*, 3098.

(43) Perdew, J. P. *Phys. Rev. B* **1986**, *33*, 8822; *34*, 7406.

(44) Lee, C.; Yang, W.; Parr, R. G. *Phys. Rev. B* **1988**, *37*, 785.

(45) Becke, A. D. *J. Chem. Phys.* **1993**, *98*, 5648.

(46) Perdew, P.; Burke, K.; Ernzerhof, M. *Phys. Rev. Lett.* **1996**, *77*, 3865−3868.

(47) Allinger, N. L. *J. Am. Chem. Soc.* **1989**, *111*, 8551.

(48) Weiner, S. J.; Kollman, P. A.; Case, D. A.; Singh, U. C.; Caterina, G.; Alagona, G.; Profeta, J. C.; Weiner, P. A. *J. Am. Chem. Soc.* **1984**, *106*, 765−784.

(49) Weiner, S. J.; Kollman, P. A.; Nguyen, D. T.; Case, D. A. *J. Comput. Chem.* **1986**, *7*, 230−252.

(50) McDonald, D. Q.; Still, W. C. *Tetrahedron Lett.* **1992**, *33*, 7743−7746.

(51) Jorgensen, W. L.; Maxwell, D. S.; Tirado-Rives, J. *J. Am. Chem. Soc.* **1996**, *118*, 11225−11235.

(52) Frisch, M. J.; Trucks, G. W.; Schlegel, H. B.; Scuseria, G. E.; Robb, M. A.; Cheeseman, J. R.; Zakrzewski, V. G.; Montgomery, J. A., Jr.; Stratmann, R. E.; Burant, J. C.; Dapprich, S.; Millam, J. M.; Daniels, A. D.; Kudin, K. N.; Strain, M. C.; Farkas, O.; Tomasi, J.; Barone, V.; Cossi, M.; Cammi, R.; Mennucci, B.; Pomelli, C.; Adamo, C.; Clifford, S.; Ochterski, J.; Petersson, G. A.; Ayala, P. Y.; Cui, Q.; Morokuma, K.; Malick, D. K.; Rabuck, A. D.; Raghavachari, K.; Foresman, J. B.; Cioslowski, J.; Ortiz, J. V.; Stefanov, B. B.; Liu, G.; Liashenko, A.; Piskorz, P.; Komaromi, I.; Gomperts, R.; Martin, R. L.; Fox, D. J.; Keith, T.; Al-Laham, M. A.; Peng, C. Y.; Nanayakkara, A.; Gonzalez, C.; Challacombe, M.; Gill, P. M. W.; Johnson, B. G.; Chen, W.; Wong, M. W.; Andres, J. L.; Head-Gordon, M.; Replogle, E. S.; Pople, J. A. *Gaussian 98*, revision A.7; Gaussian, Inc.: Pittsburgh, PA, 1998.

(53) *HyperChem Release 7*; HyperCube Inc.: Gainsville, FL, 2002.

(54) Martin, J. M. L.; Van Alsenoy, C. *GAR2PED*; University of Antwerp: Antwerp, The Netherlands, 1995.

(55) Dollish, F. R.; Fateley, W. G.; Bentley, F. F. *Characteristic Raman Frequencies of Organic Compounds*; John Wiley & Sons: New York, 1973.

(56) Destrade, C.; Dupart, E.; Joussot-Dubien, M.; Garrigou-Lagrange, C. *Can. J. Chem.* **1974**, *52*, 2590−2602.

(57) Song, S.; Asher, S. A.; Krimm, S.; Shaw, K. D. *J. Am. Chem. Soc.* **1991**, *113*, 1155−1163.

(58) Lien-Vien, D.; Colthup, N. B.; Fateley, W. G.; Grasselle, J. G. *Handbook of Infrared and Raman Characteristic Frequencies of Organic Molecules*; Academic Press: New York, 1991.

(59) Fogarasi, G.; Zhou, , X.; Taylor, P. W.; Pulay, P. *J. Am. Chem. Soc.* **1992**, *114*, 8191−8201.